

First-order and continuous melting in a two-dimensional system: Monolayer xenon on graphite

P. Dimon*

Department of Physics, University of Chicago, Chicago, Illinois 60637

P. M. Horn

IBM Thomas J. Watson Research Center, P.O. Box 218, Yorktown Heights, New York 10598

M. Sutton and R. J. Birgeneau

Department of Physics, Massachusetts Institute of Technology, Cambridge, Massachusetts 02139

D. E. Moncton

Physics Department, Brookhaven National Laboratories, Upton, New York 11973

(Received 24 May 1984)

We have performed a high-resolution x-ray scattering experiment to study the two-dimensional melting of xenon adsorbed on exfoliated graphite near the first-order-to-second-order multicritical point for coverages at and below 1 ML (ML denotes monolayer). We have crossed the liquid-solid phase boundary at three points by varying the vapor pressure at fixed temperature. At 116 K we find a weak first-order transition. At 125 and 134 K, which correspond to coverages of about 0.9 and 1.0 ML, respectively, the transition is continuous within experimental accuracy. Fits of the data in the solid phase to theories of dislocation-mediated melting yield $\eta(P_m)=0.35\pm 0.02$ at both 125 and 134 K. From hydrodynamic scaling in the liquid phase, we find $\eta(P_m)=0.24\pm 0.02$ at 116 K and $\eta(P_m)=0.23\pm 0.02$ at both 125 and 134 K. The discrepancy between the two methods for obtaining $\eta(P_m)$ cannot be simply explained. Indirect evidence for an orientationally ordered phase is also observed at 125 and 134 K through the azimuthally averaged diffraction line shapes.

I. INTRODUCTION

How does a two-dimensional solid melt? In the last decade there has been considerable success in efforts to obtain high-quality experimental data on two-dimensional (2D) systems. During the same period, significant theoretical progress has also been achieved. In particular, the dislocation-disclination unbinding model of Kosterlitz and Thouless,¹ Halperin and Nelson,² and Young³ has provided a mechanism to explain this phenomenon along with specific testable predictions. One of their main results is that the melting transition can be continuous and not first order as in three dimensions. However, some experimental results and computer simulations still strongly indicate that both types of transitions may occur in the same system, implying the existence of a multicritical point.

One important realization of a 2D melting transition is provided by rare-gas monolayers on graphite. Specifically, for xenon on graphite, Heiney *et al.* have reported a high-resolution study using synchrotron x-ray techniques of the melting transitions at coverages of 1.1 and 0.85 ML (where ML denotes monolayer). The former transition is found to be continuous within the limits imposed by the substrate heterogeneity, whereas the latter is first order. More recently, Rosenbaum *et al.* have shown that the xenon fluid is orientationally ordered. One important question which immediately arises in assessing the experiments of Heiney *et al.* is whether or not the excess coverage above 1 ML played a role in making the 1.1-ML tran-

sition continuous. More generally, one would like to understand the crossover from continuous to first-order melting as the coverage is decreased below 1 ML.

In this paper we report the results of such a study. We have again used high-resolution synchrotron x-ray-diffraction techniques; because of technical improvements we are able to make a number of statements about the correlations that are more precise than was possible at the time of the study of Heiney *et al.* We have crossed the liquid-solid phase boundary at three different temperatures by varying the three-dimensional xenon vapor pressure. The three temperatures were chosen so as to observe the first-order, the continuous, and, if possible, the multicritical region; all are at or below 1 ML coverage.

The paper has been organized in the following way: In Sec. II we outline the main features of the dislocation-disclination unbinding model of two-dimensional melting, particularly those relating to the x-ray structure factor. In Sec. III we give a summary of the experimental situation, in addition to a review of the current status of computer simulations. Section IV contains a description of the experimental setup. In Sec. V we describe some of the details of the data analysis. In Sec. VI we discuss the results of the experiment and the conclusions that may be drawn from them. Section VII is a summary of the paper. More details may be found in Ref. 4.

II. THEORY

For completeness, we review the general aspects of the theory of melting in two dimensions. Mermin⁵ has

proved that a two-dimensional crystal cannot have long-range order (LRO) except at $T=0$. However, as suggested by Stanley and Kaplan,⁶ this does not rule out the possibility of a phase transition at finite temperature between two phases, neither of which possesses LRO. Kosterlitz and Thouless¹ have proved this explicitly by showing how the 2D XY model and symmetry-equivalent models can have topological defects which mediate phase transitions. Topological defects would include vortices in a 2D superfluid or a 2D superconductor and spin vortices in the 2D XY model. In the Kosterlitz-Thouless (KT) scenario, below a critical temperature T_{KT} there will only be pairs of defects in the system. This phase will have quasi-LRO; that is, the correlations will decay algebraically with distance. At T_{KT} the pairs will begin to dissociate into free defects which establish the high-temperature disordered phase.

Later, Halperin and Nelson (HN) developed a model for the melting of a two-dimensional crystal which belongs to a different but related "universality class." In their model, as in the XY model, topological defects play an important role. However, unlike the XY model, two types of defects (dislocations and disclinations) are needed and the melting is a two-step process. Based on this model, Halperin and Nelson,² Nelson,⁷ and Young³ have extracted quantitative predictions from the original work of Kosterlitz and Thouless.¹ The major points of the 2D melting theory of Kosterlitz, Thouless, Halperin, Nelson, and Young (KTHNY) are as follows:

When $T < T_{KT}$, only bound dislocations exist in thermal equilibrium. In this phase, the crystal has positional quasi-LRO; that is, the pair-correlation function takes the form

$$C_G(\vec{R}) \sim \frac{1}{R^{\eta_G(T)}} \text{ as } R \rightarrow \infty, \quad (1)$$

so that the structure factor resembles

$$S(\vec{Q}) \sim \frac{1}{|\vec{Q}_1 - \vec{G}|^{2-\eta_G(T)}} \quad (2)$$

near a reciprocal-lattice vector \vec{G} . For a smooth substrate,

$$\eta_G(T) = \frac{k_B T G^2}{4\pi\mu_R} \frac{3\mu_R + \lambda_R}{2\mu_R + \lambda_R}, \quad (3)$$

where μ_R and λ_R are renormalized Lamé elastic constants. There is, however, LRO in the bond orientations; that is, $\langle \psi(\vec{R})\psi(\vec{0}) \rangle \rightarrow \text{const}$ as $R \rightarrow \infty$, where $\psi(\vec{R}) = e^{6i\theta(\vec{R})}$ is the bond-orientation order parameter and $\theta(\vec{R})$ is a bond angle at the site \vec{R} . As T approaches T_{KT} from below, $\eta_G(T)$ for the smallest reciprocal-lattice vector approaches a value $\eta^* = \eta(T_{KT})$, where

$$\frac{1}{4} \leq \eta^* \leq \frac{1}{3}, \quad (4)$$

depending on the specific limiting values of μ_R and λ_R near T_{KT} .

For $T_{KT} < T < T_{HN}$, the dislocation pairs begin to dissociate into free dislocations and the solid melts. There is no longer positional quasi-LRO; that is,

$$G(\vec{r}) \sim e^{-\kappa r} \text{ as } r \rightarrow \infty, \quad (5)$$

where $\kappa = \xi^{-1}$ and ξ is the correlation length. Also, at the peak Q_0 in the structure factor,

$$S(Q_0) \propto \kappa^{\eta^* - 2}, \quad (6)$$

in agreement with hydrodynamic scaling principles. The bond orientations now have quasi-LRO, i.e.,

$$\langle \psi(\vec{r})\psi(\vec{0}) \rangle \sim \frac{1}{r^{\eta_6(T)}} \text{ as } r \rightarrow \infty, \quad (7)$$

where

$$\eta_6(T) = 18k_B T / \pi K_A. \quad (8)$$

K_A is a renormalized Frank elastic constant. Since some form of bond-orientational order still persists, this has been termed an "hexatic" phase. Furthermore, as T approaches T_{KT} from above, ξ is predicted to have the unusual scaling form

$$\xi(T) = \xi_0 \exp(bt^{-\bar{\nu}}), \quad (9)$$

where b is a positive, nonuniversal constant, $t = (T - T_{KT})/T_{KT}$ is the reduced temperature, and $\bar{\nu} = 0.36963\dots$ for a smooth substrate. Note that ξ diverges at T_{KT} , indicating a continuous transition. In practice, this scaling form is probably unobservable. Greif *et al.*⁸ and Cardy⁹ have estimated the size of the critical region for the KTHNY theory and found that such a scaling law should apply only for reduced temperatures, $t < 0.01$, corresponding to correlation lengths of $\sim 10^8$ lattice spacings. (Typical experimental systems are only $\sim 10^3$ lattice spacings.)

Finally, when $T > T_{HN}$ the dislocations will dissociate into free disclinations. Now bond-orientational order is also lost (ignoring substrate effects) and one has a true liquid, i.e.,

$$\langle \psi(\vec{r})\psi(\vec{0}) \rangle \sim e^{-r/\xi_\theta}, \quad (10)$$

where ξ_θ is the bond-orientation correlation length. This transition is also continuous.

The KTHNY theory assumes that the core energy of a dislocation is large enough so that the density of dislocations is small. If the opposite were true and many dislocations were present, they could conceivably form grain boundaries. Chui¹⁰ has in fact argued that grain boundaries will always form before the dislocation pairs unbind, and that the transition would then most likely be first order.

III. PREVIOUS EXPERIMENTS

The structure of xenon on graphite has been studied by a variety of methods including adsorption isotherms,¹¹ low-energy electron diffraction (LEED), transmission high-energy electron diffraction (THEED), Auger-electron spectroscopy (AES),¹² ellipsometry,¹³ x-ray scattering,¹⁴⁻¹⁸ and hydrogen¹⁹ and helium atom scattering.²⁰ In particular, the adsorption-isotherm, LEED, THEED, and AES measurements have all reported a first-order melting transition at submonolayer coverages.

The adsorption isotherm measurements of Thomy and Duval,²¹ however, show the liquid-solid coexistence region narrowing down considerably up to their highest measured temperature, 118.1 K. Schabes-Retchkiman and Venables²² have reported that the xenon incommensurate lattice is not rotated with respect to the graphite surface,²³ although D'Amico and Moncton²⁴ have now observed this effect at higher temperatures.

The first x-ray scattering experiments of xenon on graphite were performed by Brady *et al.*,¹⁴ who observed a liquid phase at a temperature of 175 K. The melting transition was first seen by Hammonds *et al.*,¹⁵ who confirmed the existence of a 2D triple point at 99 K and found a first-order transition up to 112 K (the highest temperature they studied). As we discussed in the Introduction, more detailed experiments by Heiney *et al.*¹⁷ resulted in the observation of a continuous transition at a temperature of 152 K and a coverage of 1.1 ML. Furthermore, the data outside of the asymptotic region were well described by Eq. (9) with rescaled parameters and with $\eta \cong \frac{1}{3}$ at melting. A possible phase diagram proposed by Heiney *et al.* is shown in Fig. 1. Most recently, Rosenbaum *et al.*¹⁸ have directly observed an orientationally ordered fluid phase using exfoliated single crystals of graphite.²⁵

In addition to "real" experiments, there have also been a number of computer simulations, of both the Monte Carlo and molecular-dynamics type, which have attempted to simulate a system of interacting particles in two dimensions. The results for particles interacting with a

Lennard-Jones potential show transitions which are first order,²⁶⁻²⁸ continuous,²⁹ and ambiguous.³⁰ Many of the simulations with first-order transitions also find that there is no hexatic phase. In particular, Koch and Abraham,²⁷ and Abraham,²⁸ have specifically tried to simulate xenon on graphite, taking into account the effects of both substrate and vapor. The most recent results now appear to be consistent with this and other experiments.^{17,18}

Taking another approach, Saito³¹ has simulated a system of dislocation vectors and has found that the order of the transition depends on the size of the dislocation core energy. If the core energy is sufficiently small, dislocations will be created in large numbers and will form grain boundaries. This results in a first-order transition as predicted by Chui.¹⁰ If the core energy is too large, there will not be enough dislocations present to form grain boundaries and the transition will be continuous as predicted by the KTHNY theory. Strandburg *et al.*³² have simulated the Laplacian roughening model which is dual to the dislocation model of Saito. They find a continuous transition but cannot vary the core energy. Swendsen,³³ who has performed simulations of the 2D XY model, has found results similar to Saito regarding the core energy of a spin vortex. These particular computer experiments, then, also suggest the existence of a multicritical point.

IV. DESCRIPTION OF THE EXPERIMENT

This experiment was performed on the high-resolution setup on beam line VII-2 (wiggler line) at the Stanford Synchrotron Radiation Laboratory (SSRL). More details may be found in Ref. 34. The synchrotron produces a pulsed, highly collimated, highly-plane-polarized photon beam. It is monochromatized by a pair of parallel Ge(111) crystals which were tuned to a wavelength of 1.7548 Å corresponding to a wave vector of 3.5806 Å⁻¹. The beam then passes through a monitor counter used to normalize all counting rates since the beam intensity changes with the varying ring current. The beam size at the sample was about 2 mm × 2 mm. The scattered x rays are then analyzed by another Ge(111) crystal in the non-dispersive configuration, and finally detected by a NaI scintillation counter (also used in the monitor). The in-plane (\bar{Q}_1) resolution of this arrangement is ~ 0.0003 Å⁻¹ in both the longitudinal (radial) and transverse (angular) directions. The out-of-plane (\bar{Q}_z) resolution is ~ 0.03 Å⁻¹ near the Xe(10) peak. The sample, analyzer, and detector are all mounted on a Huber 5020 six-circle goniometer with a stepping precision of 0.0005° and an accuracy of $\sim 0.005^\circ$. The goniometer and data collection are controlled by a PDP 11/34 computer interfaced to a CAMAC electronics crate. An overall schematic of the experiment is shown in Fig. 2.

The sample itself was a piece of ZYX exfoliated graphite with dimensions 25 mm × 25 mm × 2.5 mm. The *c* axis is perpendicular to the thin plane. The crystallites of which it is comprised typically have a surface size of ~ 2000 Å (or ~ 800 lattice spacings), and a thickness of ~ 500 Å (or ~ 150 carbon layers). Thus, as has been dis-

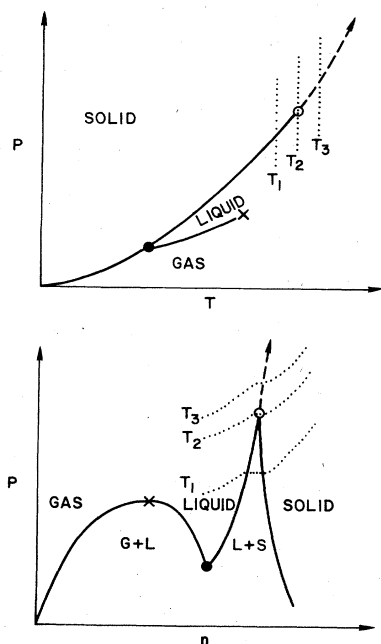


FIG. 1. Hypothetical pressure-vs-temperature and pressure-vs-density 2D phase diagrams with a multicritical point. First-order lines are solid and continuous lines are dashed. The multicritical point is shown by an open circle. The hexatic phase is not shown. The trajectories taken in the course of the present experiment are shown schematically by the dotted lines where $T_1 < T_2 < T_3$.

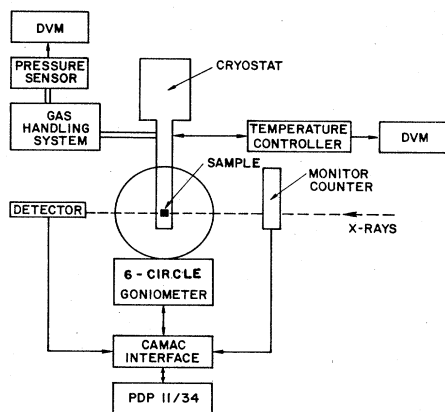


FIG. 2. Overall schematic of the experiment.

cussed extensively in the past,^{17,35} in an experiment one is not observing the scattering from a single layer of adatoms, but from many layers, each with a different but well-characterized orientation in space. Therefore, in order to compare the observed scattering intensities with theory, it is necessary to perform an orientational averaging of the appropriate theoretical structure factors, which consists of two parts: an in-plane powder average and a *c*-axis mosaic average. This will be reviewed in the next section. The in-plane powder average unfortunately compromises one's ability to study orientational ordering.

The sample was enclosed in a cylindrical sample cell which could be filled with gas from an external line. The sides of the cell were made of thin beryllium windows to allow for the passage of x rays. The cell was mounted on the end of the cold head of an Air Products Displex cryostat. A heater located on the cold-head shaft and connected to a Lakeshore DTC-500A temperature controller enabled variable-temperature regulation of the sample from ~ 15 to ~ 300 K. Both feedback and sensing were done with a calibrated silicon diode embedded in the base of the sample cell. Temperature stability was ± 20 mK over a 24-h period with an accuracy of ~ 0.1 K. The diode voltage was read from a Hewlett-Packard 3455A digital voltmeter (DVM) and the temperature was interpolated from a calibration table.

A gas-handling system controlled the amount of gas in the system. We used xenon gas with a purity of 99.995 mol %. The pressure in the system was measured by two MKS Instruments, Inc. (MKS) Baratron capacitive pressure sensors with ranges 0–10 and 0–1000 Torr, respectively. The pressure was read out directly on a Keithley 192 DVM. The precision of the (0–10)-Torr sensor was ± 0.0001 Torr with an accuracy of ~ 0.002 Torr. Using the ideal-gas law $PV = Nk_B T$, N can be determined by measuring the pressure in a known volume at a fixed temperature. Since the temperature of the gas-handling system remains fixed, the amount of gas adsorbed is most conveniently measured in units of pressure times volume, i.e., Torr cm^3 . By expanding gas into (or pumping gas out of) the system, and measuring the initial and final vapor pressures, the amount of gas adsorbed (or desorbed) can be

determined from the missing (or excess) vapor. The precision of this method was ± 0.1 Torr cm^3 with an accuracy of ~ 1 Torr cm^3 . Owing to the small diameter of the gas line in the cryostat, it was necessary to correct for thermal transpiration effects at low (< 1 Torr) pressures.³⁶

V. DATA ANALYSIS

The data analysis consisted of hypothesizing a structure factor, calculating the intensity which one would then expect to see at a detector, and then comparing this result with the data. This has been discussed by Stephens *et al.*,³⁵ but for completeness, we present the essential features here. In the solid phase, we should use the power-law structure factor, Eq. (2). In practice, we have used the modified form of Dutta and Sinha³⁷ which takes into account finite-size effects:

$$S(\vec{q}) = A_0 \Phi(1 - \frac{1}{2}\eta; 1; -q^2 L^2 / 4\pi), \quad (11)$$

where $q = |\vec{Q}_\perp - \vec{G}|$, L is the size of a crystallite, A_0 is an overall amplitude, and $\Phi(a; b; z)$ is a degenerate hypergeometric function also known as Kummer's function. [In two dimensions the scattering will only depend on the in-plane (\vec{Q}_\perp) component of the momentum transfer.] In the hexatic phase, where there is still orientational order, we shall assume for simplicity that the structure factor consists of Lorentzian spots; that is,

$$S(\vec{Q}) = \frac{A_0 \kappa^2}{(\vec{Q}_\perp - \vec{Q}_0)^2 + \kappa^2}. \quad (12)$$

Equation (12) should be an adequate approximation for the actual structure factor, when the long-range hexatic order is highly developed.¹⁸ When there are no (or weak) bond-orientational correlations, the structure factor should be isotropic. Thus in two dimensions there will be cylindrical shells of scattering, which we hypothesize to be of the simple form

$$S(\vec{Q}) = \frac{A_0 \kappa^2}{(Q_\perp - Q_0)^2 + \kappa^2}. \quad (13)$$

This form should apply to a true 2D liquid. Also, as the Lorentzian spot of the hexatic phase becomes more anisotropic away from the melting transition as bond-orientational order decreases, we expect that its structure factor will cross over from Eq. (12) to (13).

As discussed previously, due to the nature of exfoliated graphite, the theoretical structure factors must be averaged over the distribution of crystallite orientations. The in-plane powder average will smear the structure factor into a ring so that all the phases will show cylindrically symmetric scattering; that is,

$$\bar{S}(Q_\perp) \equiv \int_0^{2\pi} S[\vec{Q}'_\perp(\phi)] d\phi, \quad (14)$$

where $S[\vec{Q}'_\perp(\phi)]$ is a 2D structure factor in a primed frame that is rotated an angle ϕ relative to an unprimed reference frame. The sharp power-law peaks of the solid phase will still be apparent, although the in-plane powder average cannot be calculated analytically. As originally discussed by Hammonds *et al.*,¹⁵ if we substitute Eq. (12)

for the hexatic phase, then $\bar{S}(Q_1)$ can be evaluated exactly, yielding, to a good approximation,

$$\bar{S}(Q_1) \cong \frac{2\pi A_0 \kappa^2}{[(Q_1 - Q_0)^2 + \kappa^2]^{1/2}}. \quad (15)$$

Thus a radial scan should produce a square-root Lorentzian line shape. In the liquid phase, where the structure factor is already a ring [see Eq. (13)], the in-plane powder average will obviously have no effect. Therefore, although all explicit information on orientational order has been lost, the hexatic and liquid phases may still have different radial line shapes.

After the in-plane powder average is done, it is necessary to perform a *c*-axis mosaic average, namely

$$\tilde{S}(Q_1, Q_z) \equiv \int_0^{2\pi} d\alpha \int_0^\pi d(\cos\psi) \bar{S}(Q'_1(\alpha, \psi)) P(\psi), \quad (16)$$

where $\bar{S}(Q'_1(\alpha, \psi))$ is the in-plane powder-averaged structure factor in a primed frame that is tilted an angle ψ in a plane which makes an angle α with, for example, the Q_x - Q_z plane in the unprimed frame. $P(\psi)$ is the probability of finding a crystallite whose *c* axis is tilted an angle ψ from the mean. This distribution can be measured directly. A mosaic scan about the graphite (100) peak is shown in Fig. 3. The distribution appears to be approximately Lorentzian with a half-width at half maximum (HWHM) of 8.5° . (This must be corrected for absorption effects, after which one obtains a value of 8.3° , or 0.14 rad.)

Since the resolution of the measuring apparatus is not perfect, a resolution function $R(\vec{Q} - \vec{Q}')$ must be convoluted with the in-plane powder- and mosaic-averaged structure factor. The total intensity from a diffraction peak is then given by

$$I_{\text{diff}}(\vec{Q}) = \int d^3Q' R(\vec{Q} - \vec{Q}') |f(Q')|^2 \tilde{S}(\vec{Q}'). \quad (17)$$

The form factor $f(Q)$ has now been included. There is also a polarization factor $P(Q)$, but since synchrotron radiation is highly-plane-polarized in the orbit of the electrons, and since all further scattering of the x-ray beam (i.e., from the monochromator, sample, etc.) is in the plane perpendicular to the incident polarization vector, we may take $P(Q) = 1$. In the experiment described here, the limiting resolution factor is not the apparatus resolution ($\sim 0.0003 \text{ \AA}^{-1}$, or $\sim 3000 \text{ \AA}$), but rather the finite size of

the crystallites ($\sim 2000 \text{ \AA}$). Furthermore, the out-of-plane (Q_z) resolution will be unimportant if

$$\frac{1}{2} \frac{(\delta Q_z)^2}{G} \ll \sigma_{\text{HWHM}}, \quad (18)$$

where δQ_z is the out-of-plane resolution, G is the magnitude of the reciprocal-lattice vector of the scattering peak, and σ_{HWHM} is the half-width at half maximum of the peak. In this experiment, $\delta Q_z \cong 0.03 \text{ \AA}^{-1}$, $G \cong 1.6 \text{ \AA}^{-1}$, and $\sigma_{\text{HWHM}} \cong 0.003 \text{ \AA}^{-1}$, so that this condition is satisfied. It is therefore a valid approximation to treat the resolution as perfect and take $R(\vec{Q} - \vec{Q}') = \delta^3(\vec{Q} - \vec{Q}')$ so that

$$I_{\text{diff}}(\vec{Q}) = |f(Q)|^2 \tilde{S}(Q_1, Q_z). \quad (19)$$

There are also other sources of scattering to be considered in addition to diffraction from the adsorbate. These will all contribute to an overall background intensity $I_{\text{back}}(\vec{Q})$. There is scattering from the graphite substrate (~ 400 counts per 5×10^4 monitor counts) which can be measured directly in the absence of any adsorbate. This is by far the largest source of background. There is scattering from the 3D vapor coexisting with the adsorbed phases. Even in the worst case (largest vapor pressure), this is quite small (~ 8 counts per 5×10^4 monitor counts at a vapor pressure of 10 Torr) compared to the substrate scattering and can be neglected. All other sources of background are totally negligible.

As discussed by Heiney *et al.*, the presence of any adsorbate or vapor also results in additional absorption of the x-ray beam, which must be corrected for.¹⁷ The total calculated intensity must be multiplied by a factor $B = e^{-\mu \rho l}$ for each absorber, where μ is the mass absorption coefficient of the absorbing medium at the wavelength of the incident radiation, ρ is the mass density of the absorber, and l is the path length through the absorber. For a typical total amount adsorbed of 400 Torr cm^3 , absorption by the adatoms yields $B \cong 0.82$; thus this is a significant effect. Absorption by the xenon vapor in the sample cell was found to be negligible.

The final calculated intensity is then given by

$$I_{\text{calc}}(\vec{Q}) = B [I_{\text{diff}}(\vec{Q}) + I_{\text{back}}(\vec{Q})]. \quad (20)$$

The data analysis consisted of performing least-squares fits of the measured intensities to the calculated intensities. It should be emphasized that for each phase only three parameters were adjustable: peak amplitude, peak position, and η or κ , depending on the line shape used. A best value for the sample size L [necessary for the solid fits; see Eq. (11)] was first determined by least-squares analysis and then fixed. All other parameters (e.g., absorption factor, mosaic width) were either calculated *a priori* or directly measured.

VI. EXPERIMENTAL RESULTS

The melting transition of xenon on graphite was studied as a function of vapor pressure with the temperature of the graphite sample held fixed. This was done at three temperatures, 116, 125, and 134 K, which were estimated

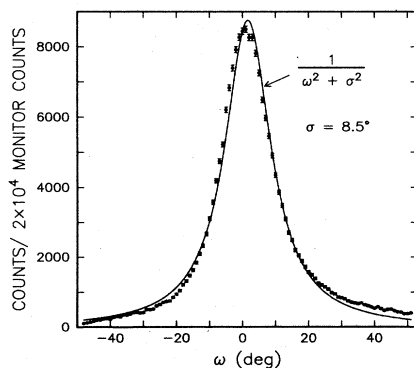


FIG. 3. Rocking curve of the (100) peak in ZYX graphite showing the *c*-axis mosaic distribution. The solid curve is a fit to a Lorentzian line shape. (5×10^4 monitor counts is ~ 5 sec.)

from the Thomy-Duval¹¹ isotherm data to be in the first-order, multicritical, and continuous regions, respectively (see Fig. 1). Thus, at each temperature, we also have *in situ* adsorption isotherms. Unfortunately, these were not as clean as we would have liked, possibly due to capillary condensation.³⁸ Adsorption isotherms of xenon on graphite taken more carefully after the completion of the x-ray experiment are shown in Fig. 4. We will show below that the melting transitions at 116, 125, and 134 K are at pressures (P_m) of 0.0405, 0.305, and 2.05 Torr, respectively. The first of these pressures is too low for the transition to be observable in the isotherm in Fig. 4. At 125 K there is an inflection in the isotherm which is approximately at the P_m . By 134 K the inflection in the isotherm has become quite broad and is at a pressure slightly below P_m . Unfortunately, because the isotherms were not carried out coincidentally with the scattering experiments, we cannot rule out slight systematic errors in the absolute values of the transition pressures. Point B_1 is the conventional definition of 1 ML which was found to be (535 ± 10) Torr cm^2 . The coverage in these units at the melting transitions at 116, 125, and 134 K are 0.86, 0.88, and 1.0 ML, respectively. It should be emphasized, however, that since there is no unique way of defining a monolayer, these numbers are subject to systematic errors.

At each vapor-pressure point, a radial x-ray scan was performed from 1.3 to 1.8 \AA^{-1} , with a more detailed scan taken near the peak if it was sharp. Scans were taken repeatedly as the system approached equilibrium. Thus, when the vapor-pressure and x-ray intensities stopped changing, we could be reasonably sure that equilibrium had been achieved. Also, as a further test, the system was periodically thermally shocked to see if it would return to the same equilibrium conditions as before the shock,

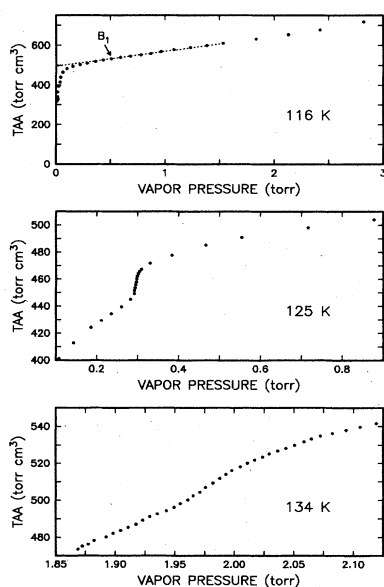


FIG. 4. Adsorption isotherms of xenon on graphite. The melting transition is evident at 125 K and is seen as a small inflection at 134 K. There is not enough detail to see it in the 116-K data. Point B_1 is the conventional definition of 1 ML. The error bars are smaller than the size of the points.

which it did. A summary of the melting (or actually freezing) sequence at 134 K is shown in Fig. 5. The data have been background-subtracted, leaving only the signal from the adsorbed layer. An attempt was made to fit each scan to each of the three postulated line shapes: a Lorentzian spot (LOR SPOT), a Lorentzian ring (LOR RING), and a Kummer function (KUMMER). It is revealing to plot the normalized χ -squared values for each fit as a function of vapor pressure, as shown in Fig. 6. At 125 and 134 K the Lorentzian-ring fits work best at low pressures, the Lorentzian-spot fits work best in some intermediate region, and both the Kummer-function and Lorentzian-spot fits work almost equally well at high pressures. (This is not too surprising, since for a very sharp peak, a Lorentzian spot is mostly power-law tail anyway.) At 116 K there does not seem to be a region where the Lorentzian-spot structure factor works best. By fitting the central peaks of the data that are clearly in the solid phase to the Kummer function, a best value for L of 2300 \AA was determined.

The ability to distinguish a Lorentzian ring from a Lorentzian spot is demonstrated in Fig. 7. The fact that, at 125 and 134 K, the Lorentzian spot works better in some small region that either a Lorentzian ring or a Kummer function implies that the original assumption of an orientationally ordered phase is correct. Thus, we have indirect evidence for the hexatic phase close to T_c . An orientationally ordered fluid has now been directly observed by Rosenbaum *et al.*¹⁸ Although no Lorentzian-spot fits were found to work best at 116 K, there are not enough data points to rule out the existence of the hexatic phase at that temperature.

At 116 K, under the assumption that the transition is first order, and that there is therefore a coexistence region, fits to a sum of a Kummer function and a Lorentzian spot were attempted. (This assumes the existence of the hexatic phase. Using a Lorentzian ring instead made little

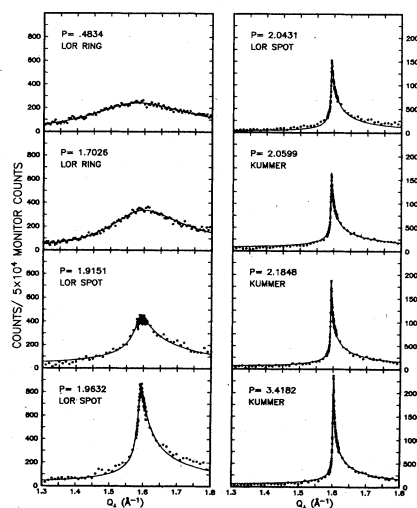


FIG. 5. X-ray scans of the Xe(10) peak at 134 K. The pressures are in Torr. The error bars have been omitted for the sake of clarity. The solid lines are fits to the data as explained in the text.

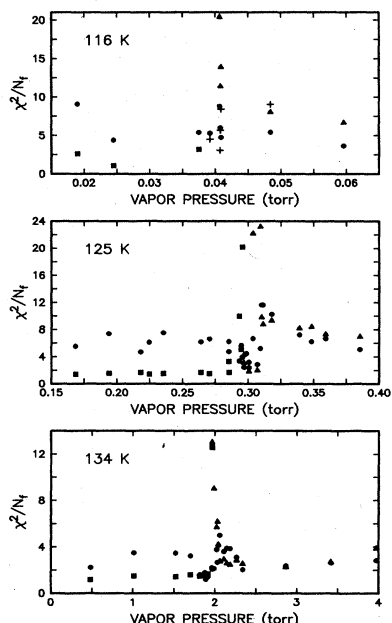


FIG. 6. Normalized χ -squared values as a function of vapor pressure for Lorentzian-ring fits (■), Lorentzian-spot fits (●), Kummer fits (▲), and coexistence fits (+).

difference in the qualitative results.) Since only the peak amplitudes should vary in a coexistence region, these fits were made with κ and η held fixed at their estimated values on the liquid and solid phase boundaries, respectively. The positions of the peaks were allowed to vary as a consistency check. (The same analysis was performed on the 125-K data, but since there is no obvious coexistence region at that temperature, there is no way to assign values to the fixed variables.) An example of a coexistence fit is shown in Fig. 8. In some cases this proved to be a better fit than either a Kummer-function or a Lorentzian-spot fit alone. Further evidence that the tran-

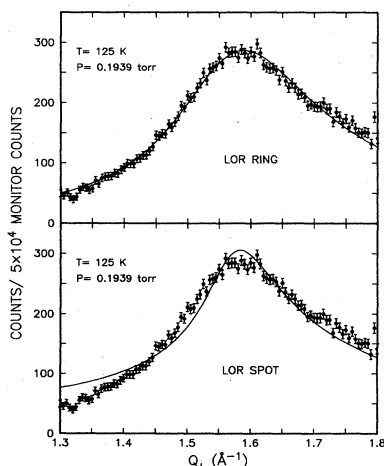


FIG. 7. Comparison of a Lorentzian-ring fit and a Lorentzian-spot fit for the same scan. In the Lorentzian-ring fit, $\kappa=0.1166 \text{ \AA}^{-1}$, and in the Lorentzian-spot fit, $\kappa=0.0475 \text{ \AA}^{-1}$.

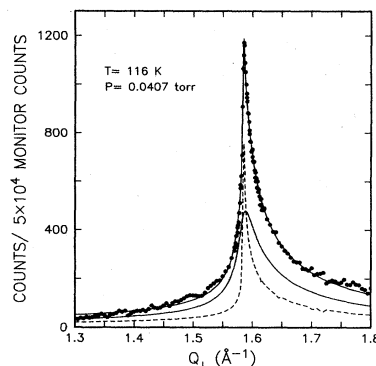


FIG. 8. Coexistence fit at 116 K. The line through the points is the sum of the dashed line (Kummer function) and the solid line (Lorentzian spot). In this example, $G=1.58440 \text{ \AA}$, $Q_0=1.5860 \text{ \AA}$, $\kappa=0.00864 \text{ \AA}^{-1}$, and $\eta=0.25$.

sition at 116 K is first order may be seen in Fig. 9. This shows a plot of the measured peak intensity as a function of vapor pressure. There is a discontinuous jump at the melting pressure P_m . This may be interpreted as the solid peak growing out of the liquid peak in the coexistence region where the pressure is constant. It is clear, however, from the large correlation length of the liquid at the transition, that at 116 K the freezing is only weakly first order. This agrees with the 54-\AA correlation length determined by Hammonds *et al.*¹⁵

The fits yield values for the melting pressure of $P_m=(0.0405\pm 0.005)$ Torr at 116 K, (0.305 ± 0.004) Torr at 125 K, and (2.05 ± 0.01) Torr at 134 K. As we have noted previously, the melting transition at both 116 and 125 K is well below 1 ML. At 134 K it seems to occur at or just below above 1 ML.

Several features of the data should be noted at this point. First, there is no evidence in the solid phase at these temperatures for satellite peaks produced by the modulation of the adsorbate lattice by the substrate field. These should occur at linear combinations of adsorbate and substrate reciprocal-lattice vectors. Thus, for a xenon superlattice rotated 30° with respect to the substrate, there should be a primary modulation peak at 1.75 \AA^{-1} coming from the Xe(10) reciprocal-lattice vector at 1.6 \AA^{-1} and the graphite (100) reciprocal-lattice vector at 2.946 \AA^{-1} .

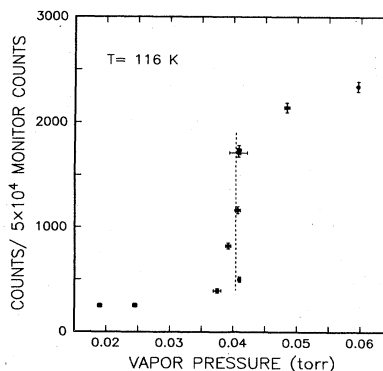


FIG. 9. Peak intensity as a function of vapor pressure at 116 K.

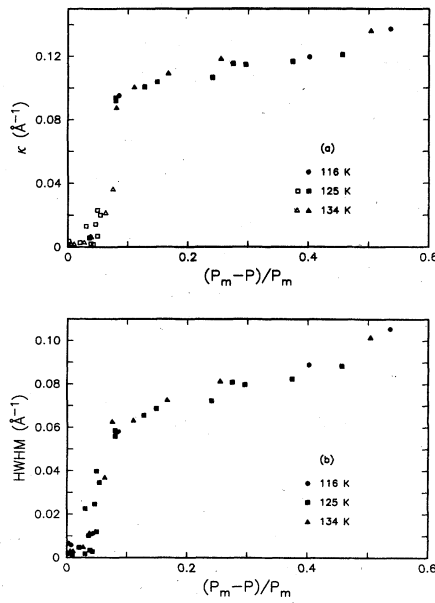


FIG. 10. (a) Fitted κ and (b) HWHM of the peaks as a function of reduced pressure. The open symbols are from the Lorentzian-spot fits and the solid symbols are from the Lorentzian-ring fits. The error bars are approximately the size of the points.

No such signal is observed. Second, the solid scans seem to deviate slightly from the predicted power-law behavior, particularly on the low- Q_{\perp} side, but since the theory was derived in the limit of large R or small q , it should break down when $q \sim 1/a$. Third, in principle, η should vary as Q^2 ,³⁹ but in this analysis it was taken to be independent of Q . [In the KTHNY theory, it is always assumed that one is very near a reciprocal-lattice vector, so that in Eq. (3) they have fixed $Q=G$.] Fits were tried with a Q^2 -dependent η , but this had little effect on the results, not surprisingly, since all the statistical weight is in the peak anyway.

The values for κ at all three temperatures, obtained

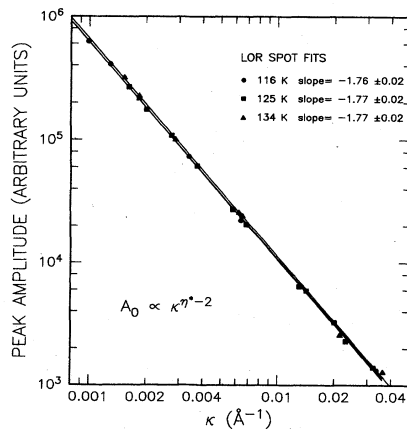


FIG. 11. Peak amplitude A_0 vs κ from the Lorentzian-spot fits on a double-logarithmic plot. The error bars are approximately the size of the points.

from the best fits, are plotted in Fig. 10(a) as a function of reduced pressure $(P_m - P)/P_m$. Thus, at low pressures they are all from the Lorentzian-ring fits, and at higher pressures, but still in the liquid phase, they are all from the Lorentzian-spot fits. The data appear to scale even though they are all outside of the KTHNY asymptotic region. Because of the change in line shape there is an apparent jump in κ from ~ 0.004 to $\sim 0.010 \text{ \AA}^{-1}$. This is clearly an artifact since the intrinsic line shape must evolve continuously. To give a better indication of the actual evolution, we plot in Fig. 10(b) the fitted HWHM. The concave curvature near the transition may be real, although we cannot rule out inhomogeneities in the graphite surface. However, it probably does not reflect the asymptotic form for $\kappa(T)$ from the KTHNY theory [see Eq. (9)]. (It should be noted here that, whereas all the predictions in Sec. II were given as a function of temperature, in this experiment we have studied everything as a function of pressure. Nevertheless, the results should be the same.) The data shown in Fig. 10 are quite similar to those obtained by Heiney *et al.* at 152 K. One of the most interesting features of the data is that the actual transition region is extremely narrow. By way of comparison, for the nearest-neighbor 2D XY model for a comparable change in K, the temperature scale is expanded by more than an order of magnitude.⁴⁰ This compression is to be expected for two reasons. First, the existence of hexatic (bond-angle) correlations will rescale the bare lengths, thereby increasing ξ_0 and decreasing b [Eq. (9)] from their values in the XY model. Second, all temperatures studied are in the vicinity of the multicritical point at which the transition becomes first order. Indeed, the surprising fact that the data scale with reduced pressure suggests an extremely gradual crossover (large crossover exponent) as one moves away from the multicritical point.

From the Lorentzian-spot fits we may obtain a value for η^* from the hydrodynamic scaling relation $A_0 \propto \kappa^{\eta^*-2}$ [see Eqs. (6) and (12)]. A plot of A_0 versus κ on a double-logarithmic scale is shown in Fig. 11 for all three temperatures. The values obtained are $\eta^* = 0.24 \pm 0.02$ at 116 K, and $\eta^* = 0.23 \pm 0.02$ at 125 and 134 K. (Notice, however, only three points exist in the liquid phase at 116

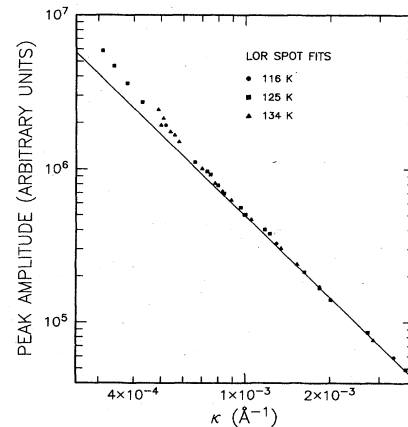


FIG. 12. Lorentzian-spot fits continued into the solid phase showing the breakdown of hydrodynamic scaling. The straight line has been extrapolated from Fig. 11.

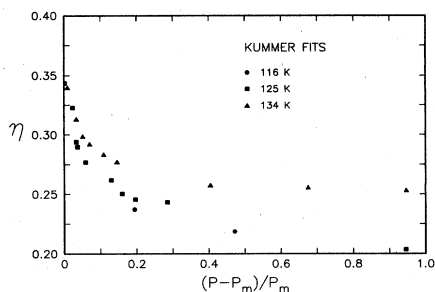


FIG. 13. η as a function of reduced pressure from Kummer-function fits. The error bars are approximately the size of the points.

K.) These may be compared to the value of $\eta^* = 0.28 \pm 0.05$ obtained by Heiney *et al.*¹⁷ using the same method. In Fig. 12 the same data are shown, but with fits to a Lorentzian spot extended into the solid phase as well. Near the melting transition the fitted values deviate from the straight lines shown in Fig. 12 extrapolated to smaller κ . (Only one line is shown for clarity.) Thus, even though the Lorentzian spot works equally well as the Kummer fits in the solid phase, this breakdown in the scaling relationship is an indication that a Lorentzian spot is no longer the correct line shape.⁴¹ The correctness of the Kummer-function line shape in the solid phase can be directly illustrated by noting how the observed scattering depends on the instrumental resolution.¹⁷ It should be noted that the Lorentzian-spot fits from 116 K have been included in Figs. 11 and 12. Why they should follow the

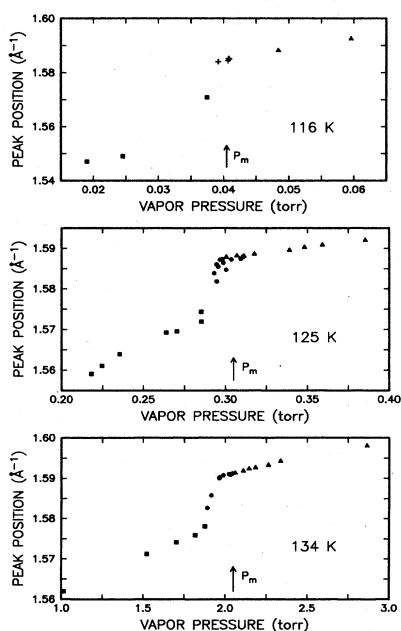


FIG. 14. Peak positions from the best fits: Lorentzian ring (■), Lorentzian spot (●), Kummer function (▲), and the solid peak from the coexistence fits (+). The error bars are approximately the size of the points.

universal curve is a mystery since the transition is first order, and, moreover, they are not the best fits. This may, however, be just another indication that the transition has a large crossover exponent. The values of κ from the Lorentzian-ring fits do not scale, but this is to be expected when $\kappa \sim 1/a$.

Values for η may also be obtained from fits to the Kummer function, Eq. (11), in the solid phase. The results are shown in Fig. 13 as a function of reduced pressure. These results are quite similar to those obtained by Heiney *et al.*¹⁷ At both 125 and 134 K, η approaches a value of $\eta^* = 0.35 \pm 0.02$ at the melting transition, a number rather different from that obtained above from hydrodynamic scaling on the liquid side. At present, this discrepancy is not understood. There could be some systematic error in η^* determined either by hydrodynamic scaling or from the line-shape analysis. In either case, it appears that additional theoretical input is called for. Unfortunately, there are not enough data at 116 K to determine η^* .

Finally, the peak positions from all the best fits are plotted in Fig. 14 for each temperature. In a first-order transition the peak position of each phase would remain unchanged as the vapor pressure was increased. This appears to be the case for the solid peaks in the coexistence fits at 116 K. Certainly at 134 K the peak position changes smoothly and monotonically. The data at 125 K are not as clean.

VII. SUMMARY

We have examined the melting of xenon on graphite at three temperatures, 116, 125, and 134 K, as a function of vapor pressure. At 116 K the transition is weakly first order, as evidenced by a jump in the peak intensity at the transition pressure, the ability to fit to coexistence line shapes, and a solid peak position that does not change significantly in the coexistence region. At 125 and 134 K the transition is continuous within our experimental accuracy; all quantities change smoothly as a function of vapor pressure and there is no apparent coexistence region. Values for η^* have been obtained from hydrodynamic scaling at all three temperatures. We find that $\eta^* = 0.24 \pm 0.02$ at 116 K, and $\eta^* = 0.23 \pm 0.02$ at 125 and 134 K. Indeed, the inverse correlation lengths at all three temperatures follow a universal law as a function of reduced pressure, even though the data are taken well outside the asymptotic critical region^{8,9} and the transition at 116 K is first order. Values for η^* have been obtained from fits in the solid phase. We find that $\eta^* = 0.35 \pm 0.02$ at 125 and 134 K. These values disagree somewhat with the results from hydrodynamic scaling and this remains a mystery. All the results, however, are still within the bounds of the KTHNY theory and are consistent with the experiments of Heiney *et al.*¹⁷

It appears that we have indirectly seen an orientationally ordered fluid phase at 125 and 134 K by observing a crossover in the best fits from a Lorentzian-ring line shape to a Lorentzian-spot line shape.

The crossover from a first-order transition at 116 K to

a continuous transition is remarkably gradual. For example, the transition at 125 K is essentially identical to the transitions at 134 and 152 K, while the transition at 116 K is quite weakly first order. We found this very surprising since we initially anticipated dramatic effects in the multicritical region.

It is certainly clear that the melting of xenon on graphite can be either first order or continuous, depending on where one crosses the phase boundary, and hence, the density at melting. This may be connected with the computer simulations of Saito³¹ and Swendsen,³³ which indicate that the dislocation core energy must play a role in the physics of 2D melting. However, there is an urgent need for a renewed theoretical effort to examine the crossover from first- to second-order melting in physically relevant models. Hopefully, the results reported in this paper will provide an appropriate testing ground for such theories.

ACKNOWLEDGMENTS

It is a pleasure to acknowledge helpful discussions with Geoff Grinstein, Bob Suter, Pulak Dutta, Steve Nagler, Robijn Bruinsma, Bob Pelcovits, John Toner, and Sunil Sinha. We also thank the staff at SSRL for their kind assistance. The work at the Massachusetts Institute of Technology was supported by the U.S. Army Research Office under Contract No. DAAG-29-81-0029 and by the National Science Foundation Materials Research Laboratory under Contract No. DMR-81-19295; work at Brookhaven National Laboratory was supported by the U.S. Department of Energy under Contract No. DE-AC02-76CH00016. One of us (P.D.) would like to thank IBM for providing financial support during his stay at the T. J. Watson Research Center. Another of us (M.S.) would like to acknowledge a NATO fellowship.

*Present address: Corporate Research Science Laboratory, Exxon Research and Engineering Co., Annandale, New Jersey 08801.

¹J. M. Kosterlitz and D. J. Thouless, *J. Phys. C* **5**, L124 (1972); **6**, 1181 (1973). See also V. L. Berezinskii, *Zh. Eksp. Teor. Fiz.* **59**, 907 (1970); **61**, 1144 (1970) [*Sov. Phys.—JETP* **32**, 493 (1971); **34**, 610 (1972)].

²B. I. Halperin and D. R. Nelson, *Phys. Rev. Lett.* **41**, 121 (1978); 519 (1978); D. R. Nelson and B. I. Halperin, *Phys. Rev. B* **19**, 2457 (1979).

³A. P. Young, *Phys. Rev. B* **19**, 1855 (1979).

⁴P. Dimon, Ph.D. thesis, University of Chicago, 1984.

⁵N. D. Mermin, *Phys. Rev.* **176**, 250 (1968).

⁶H. E. Stanley and T. A. Kaplan, *Phys. Rev. Lett.* **17**, 913 (1966).

⁷D. R. Nelson, *Phys. Rev. B* **18**, 2318 (1978).

⁸J. M. Greif, D. L. Goodstein, and A. F. Silva-Moreira, *Phys. Rev. B* **25**, 6838 (1982).

⁹J. L. Cardy, *Phys. Rev. B* **26**, 6311 (1982).

¹⁰S. T. Chui, *Phys. Rev. Lett.* **48**, 933 (1982); *Phys. Rev. B* **28**, 178 (1983).

¹¹C. F. Prenzlow and G. D. Halsey, Jr., *J. Phys. Chem.* **61**, 1158 (1957); J. R. Sams, Jr., G. Constabaris, and G. D. Halsey, Jr., *ibid.* **64**, 1689 (1960); A. Thomy and X. Duval, *J. Chim. Phys.* **66**, 1966 (1969); **67**, 286 (1970); 1101 (1970); A. Thomy, J. Régnier, J. Menaucourt, and X. Duval, *J. Cryst. Growth* **13–14**, 159 (1972); J. Régnier, A. Thomy, and X. Duval, *J. Chim. Phys.* **74**, 926 (1977). For a review, see A. Thomy, X. Duval, and J. Régnier, *Surf. Sci. Rep.* **1**, 1 (1981).

¹²J. Morrison and J. J. Lander, *Surf. Sci.* **5**, 163 (1966); J. J. Lander and J. Morrison, *ibid.* **6**, 1 (1967); J. Suzanne, G. Albinet, and M. Bienfait, *J. Cryst. Growth* **13–14**, 164 (1972); J. Suzanne, J. P. Coulomb, and M. Bienfait, *Surf. Sci.* **40**, 414 (1973); **44**, 141 (1974); **47**, 204 (1975); J. P. Coulomb, J. Suzanne, M. Bienfait, and P. Masri, *Solid State Commun.* **15**, 1585 (1974); J. Suzanne, J. P. Coulomb, and M. Bienfait, *J. Cryst. Growth* **31**, 87 (1975); J. A. Venables, H. M. Kramer, and G. L. Price, *Surf. Sci.* **55**, 373 (1976); **57**, 782 (1976); M. Bienfait and J. A. Venables, *ibid.* **64**, 425 (1977); J. Suzanne and M. Bienfait, *J. Phys. (Paris) Colloq.* **38**, C4-93 (1977); J. A. Venables and P. S. Schabes-Retchkiman, *ibid.* **38**, C4-105 (1977); P. S. Schabes-Retchkiman and J. A. Venables, *Surf. Sci.* **105**, 536 (1981).

¹³G. Quentel, J. M. Rickard, and R. Kern, *Surf. Sci.* **50**, 343 (1975).

¹⁴G. W. Brady, D. B. Fein, and W. A. Steele, *Phys. Rev. B* **15**, 1120 (1977).

¹⁵E. M. Hammonds, P. Heiney, P. W. Stephens, R. J. Birgeneau, and P. Horn, *J. Phys. C* **13**, L301 (1980).

¹⁶R. J. Birgeneau, E. M. Hammonds, P. Heiney, P. W. Stephens, and P. M. Horn, in *Ordering in Two Dimensions*, edited by S. K. Sinha (North-Holland, New York, 1980).

¹⁷P. A. Heiney, R. J. Birgeneau, G. S. Brown, P. M. Horn, D. E. Moncton, and P. W. Stephens, *Phys. Rev. Lett.* **48**, 104 (1982). P. A. Heiney, P. W. Stephens, R. J. Birgeneau, P. M. Horn, and D. E. Moncton, *Phys. Rev. B* **28**, 6416 (1983). See also P. A. Heiney, Ph.D. thesis, Massachusetts Institute of Technology, 1982.

¹⁸T. F. Rosenbaum, S. E. Nagler, P. M. Horn, and R. Clarke, *Phys. Rev. Lett.* **50**, 1791 (1983).

¹⁹T. H. Ellis, S. Iannotta, G. Scoles, and U. Valbusa, *Phys. Rev. B* **24**, 2307 (1981).

²⁰G. Bracco, P. Cantini, A. Glachant, and R. Tatarek, *Surf. Sci.* **125**, L81 (1983).

²¹A. Thomy and X. Duval, *J. Chim. Phys.* **67**, 1101 (1970).

²²See P. S. Schabes-Retchkiman and J. A. Venables, Ref. 12.

²³A. D. Novaco and J. P. McTague, *Phys. Rev. Lett.* **38**, 1286 (1977); J. P. McTague and A. D. Novaco, *Phys. Rev. B* **19**, 5299 (1979).

²⁴K. D'Amico and D. E. Moncton (private communication).

²⁵R. Clarke, P. M. Horn, S. E. Nagler, and T. F. Rosenbaum, *J. Appl. Phys.* **55**, 1231 (1984).

²⁶See, for example, R. M. J. Cotterill and L. B. Pedersen, *Solid State Commun.* **10**, 439 (1972); F. Tsien and J. P. Valleau, *Mol. Phys.* **27**, 177 (1974); S. Toxvaerd, *ibid.* **29**, 373 (1975); *J. Chem. Phys.* **69**, 4750 (1978); *Phys. Rev. Lett.* **44**, 1002 (1980); *Phys. Rev. A* **24**, 2735 (1981); F. F. Abraham, *Phys. Rev. Lett.* **44**, 463 (1980); *Phys. Rep.* **80**, 339 (1981).

²⁷S. W. Koch and F. F. Abraham, *Phys. Rev. B* **27**, 2964 (1983).

²⁸F. F. Abraham, *Phys. Rev. Lett.* **50**, 978 (1983); *Phys. Rev. B* **29**, 2606 (1984).

²⁹D. Frenkel and J. P. McTague, *Phys. Rev. Lett.* **42**, 1632 (1979).

³⁰J. Tobochnik and G. V. Chester, *Phys. Rev. B* **25**, 6778 (1982);

- S. Toxvaerd, Phys. Rev. Lett. **51**, 1971 (1983).
- ³¹Y. Saito, Phys. Rev. Lett. **48**, 1114 (1982); Phys. Rev. B **26**, 6239 (1982).
- ³²K. J. Strandburg, S. A. Solla, and G. V. Chester, Phys. Rev. B **28**, 2718 (1983).
- ³³R. H. Swendsen, Phys. Rev. Lett. **49**, 1302 (1982).
- ³⁴D. E. Moncton and G. S. Brown, Nucl. Instrum. and Methods **208**, 579 (1983).
- ³⁵P. W. Stephens, P. A. Heiney, R. J. Birgeneau, P. M. Horn, D. E. Moncton, and G. S. Brown, Phys. Rev. B **29**, 3512 (1984).
- ³⁶See T. Takaishi and Y. Sensui, Trans. Faraday Soc. **59**, 2503 (1963).
- ³⁷P. Dutta and S. K. Sinha, Phys. Rev. Lett. **47**, 50 (1981).
- ³⁸J. Chalupa and B. A. Huberman, J. Chem. Phys. **72**, 5276 (1980).
- ³⁹See, for example, B. Jancovici, Phys. Rev. Lett. **19**, 20 (1967); Y. Imry and L. Gunther, Phys. Rev. B **3**, 3939 (1971); Y. Imry, CRC Crit. Rev. Solid State Mater. Sci. **8**, 157 (1979).
- ⁴⁰The overall temperature dependence of the XY-model correlation length can be obtained by a renormalization-group matching technique [S. Heinekamp and R. Pelcovitz (private communication)].
- ⁴¹This test has been previously employed by P. Dutta, S. K. Sinha, P. Vora, M. Nielsen, L. Passell, and M. Bretz, in *Ordering in Two Dimensions*, Ref. 16.